Chirality determination in crystals

Ángela Valentín-Pérez, Patrick Rosa, Elisabeth A. Hillard, Michel Giorgi

Chirality determination in crystals

Ángela Valentín-Pérez,[1,2] Patrick Rosa,[1,2] Elizabeth A. Hillard,[1,2] Michel Giorgi[3]

1 CNRS, Univ. Bordeaux, Bordeaux INP, ICMCB, UMR, F-33600 Pessac, France

2 Univ. Bordeaux, ICMCB, UPR 9048, F-33600 Pessac, France

3 Aix Marseille Univ, CNRS, Centrale Marseille, Spectropole FR1739, Marseille, France

Corresponding author : patrick.rosa@icmcb.cnrs.fr

Abstract: This tutorial review article discusses chirality determination in the solid state, both in single crystals and in crystal assemblies, with an emphasis on X-ray diffraction. The main principles of using X-ray diffraction to reliably determine absolute structure are summarized, and the complexity which can be encountered in chiral structures – kryptoracemates, scalemates and inversion twinning – is illustrated with examples from our laboratories and the literature. We then address the problem of the bulk crystallization and discuss different techniques to determine chirality in a large assembly of crystal structures, with a special prominence given to an X-ray natural circular dichroism mapping technique that we recently reported.

1. Introduction

The study of crystalline chiral materials is of increasing interest in many fields of science ([1,2] and articles cited within), and therefore a reliable determination of their handedness is of prime importance. Depending on the field of study, the desired information will differ. For instance, the chemist will be more concerned by the determination of the absolute configuration of the compound of interest (asymmetric catalysis, pharmaceuticals…), while the physicist will seek to characterize the absolute structure of the crystal in order to relate it to its properties (chiroptics, photonics…). There are few methods that allow a direct description of chirality in either the liquid or solid state. Chiroptical spectroscopy, and more particularly circular dichroism (CD), is one of them, and is very efficient in the first case, but is confronted with many difficulties in the second case. This is notably because of the problem of birefringence [3,4], thus requiring more complicated techniques like Mueller Matrix Spectroscopy. NMR can also provide valuable information in the liquid or solid state on the chirality of the compounds studied, for instance by using chiral resolving agents [5,6]. On the other hand, solid state NMR can probe crystal packing and specific interactions to discriminate racemic or enantiopure powders or single crystals by comparing the isotropic chemical shifts of the samples [7]. However, in

none of these cases is the determination of the correct handedness of the compound or material trivial or direct.

Single crystal X-ray diffraction (SCXRD) doesn't suffer from all these drawbacks. Along with electron and neutron diffraction, SCRXD is one of the main diffraction techniques used to determine crystal structures at the atomic scale. Each of these irradiation sources has its own advantages and disadvantages, but are all capable of characterizing the handedness, in a broad sense, of a chiral material. The specificity of neutron diffraction is that it allows the study of magnetic chirality, which is a very important area in material science, but this is not the purpose of the present article and will not be developed here [8,9]. Single crystal neutron diffraction can also be used to determine the absolute configuration of chemical compounds, using a co-crystallized chiral reference [10,11], or through anomalous scattering of targeted isotopes embedded in the molecule of interest [12,13]. However, these methods have not been widely used, mainly because of their complexity, as they require large crystals, not easily-accessible neutron sources, and suffer from a limitation of the number of usable isotopes and very high absorption of most of them.

Until recently, the use of electron diffraction data for the refinement of crystal structures was considered as too complex to compete with X-ray and neutron diffraction [14,15]. Indeed, although it has the advantage of being able to analyze crystals of nanometric size thanks to the strong electron/matter interaction, the kinematic approximation used until recently made the treatment of the diffracted intensity more complicated than in the case of the two other sources. However, by considering the dynamic conditions of diffraction (multiple scattering of diffracted electrons), combined with the development of the electron precession technique and adapted software, some pioneers have opened the way to a new era in this field and particularly in nanocrystallography [16,17]. These new developments should also allow in principle the determination of the absolute structure of a crystal by taking into account the dynamic effects of electron diffraction. But the technique faces several problems, notably, in organic compounds. Here, the presence of weak scatterers induces only a weak dynamic diffraction effect, and the data can suffer a loss of resolution due mainly to the damage induced by the incident beam on the crystal. Some nice results could however be obtained using this methodology, which is still under development [18–20].

The most commonly used method for absolute structure and configuration determination remains SCXRD because it is the most established, is accessible in the laboratory, and has also benefited from the most developments over the last decades. The results obtained with this technique are sufficiently clear and precise to be able to assign the handedness of a chiral material with certainty, provided that the appropriate experimental protocols are implemented, that the entire process of structure determination and data refinement is mastered, and that it can be shown that the results obtained on the crystal are representative of the batch. But, although these points are crucial, they are not always well understood and correctly implemented. The main topic of this paper will therefore try to address these

issues. In the first section we will focus on single crystal X-ray diffraction going back to the basics of the technique by presenting the necessary conditions to determine the correct handedness of the chiral material of interest, by clarifying the vocabulary and terms needed to understand and validate the results, and by pointing out the problems and pitfalls frequently encountered in this field. In a second section, we will present a new method, X-ray Natural Circular Dichroism (XNCD) mapping, that we developed in order to investigate the crystal assemblies to try to address the problem of single crystal representativity in the bulk.

2. Fundamentals of single crystal X-ray diffraction

In the very first part of this section we go back to the fundamentals of the technique that, obviously, do not concern experienced crystallographers. However, as this article is mainly intended for students, new workers in the field and non-specialists, we thought it would be appropriate to introduce the basics of single crystal X-ray diffraction (SCXRD) for a better understanding of the notions developed later in the manuscript. SCXRD is a common technique to study the arrangement of atoms of a crystalline solid, revealing essential chemical information such as bond distances, angles, and the packing of the molecules in the solid state. The importance of XRD is reflected in the modern definition of a crystal: "*by 'crystal' we mean any solid having an essentially discrete diffraction diagram*," according to the International Union of Crystallography [21]. X-ray diffraction is based on constructive interference of monochromatic X-rays diffracted from a crystalline sample. The basis of this technique is Bragg's Law, which predicts when diffraction will take place and explains the relationship between an incident X-ray and the diffracted beams [22]. This law states that when the X-ray is incident to a crystal plane, its angle of incidence (θ) is the same as the scattering angle. When the path difference (d) is equal to an integer number (n) multiplied by the wavelength (λ), a constructive interference occurs. When n is not an integer number, the waves are not in phase and destructive interference occurs. Therefore, Bragg's law can be formulated as:

$$n\lambda = 2d\ sin\theta$$

Where λ is the wavelength of the X-ray, d is the spacing between the plane of atoms (path difference), θ is the incident angle (the angle between the incident ray and the scattering plane), and n is an integer number.

A crystal consists of a periodic, tridimensional stacking of a basic element, called the unit cell. Depending on the unit cell parameters (dimensions a, b, c, and angles α, β, and γ), seven crystal systems can be distinguished: cubic, hexagonal, tetragonal, trigonal, orthorhombic, monoclinic, and triclinic. The combination of these crystal systems with the possible centering in the cells gives the 14 Bravais lattices. The lattice centering types are primitive centering (P), body-centered (I), face-centered (F), base-

centered (*A*, *B* or *C*) and R-centered (*R*), but not all of them are allowed in all crystal systems. The permitted Bravais lattices for each crystal system are given in Table 1.

Table 1. Unit cell parameters and possible Bravais lattices for each crystal system.

Crystal system	Unit cell parameters	Possible Bravais lattices
Cubic	$a = b = c$ $\alpha = \beta = \gamma = 90$ °	*P, I, F*
Hexagonal	$a = b \neq c$ $\alpha = \beta = 90$ ° $\gamma = 120$ °	*P*
Tetragonal	$a = b \neq c$ $\alpha = \beta = \gamma = 90$ °	*P, I*
Rhombohedral	$a = b = c$ $\alpha = \beta = \gamma \neq 90$ °	*P*
Orthorhombic	$a \neq b \neq c$ $\alpha = \beta = \gamma = 90$ °	*P, I, F, C*
Monoclinic	$a \neq b \neq c$ $\alpha = \gamma = 90$ ° $\beta \neq 90$ °	*P, C*
Triclinic	$a \neq b \neq c$ $\alpha \neq \beta \neq \gamma \neq 90$ °	*P*

Ignoring symmetry operations involving translation, 32 point groups can be constructed by combining symmetry operations in three dimensional space. These 32 point groups can be divided in 21 non-centrosymmetric point groups and 11 centrosymmetric point groups, also called Laue groups. By combining the 32 point groups with the 14 Bravais lattices, 230 space groups are obtained, which take into account the translation symmetry operations.

The identification of the space group is the first step to determine if a compound is chiral. The 230 space groups can be classified into centrosymmetric (the crystal structure contains an inversion point), or non-centrosymmetric (there is not an inversion point in the crystal structure). In the second category, the space groups can be divided once more in Sohncke or non-Sohncke space groups [23]. The non-Sohncke space groups contain symmetry operations of the second kind (namely mirror planes and roto-inversions), while the Sohncke space groups contain only symmetry operations of the first kind (rotations and translations). It is important to note that a chirally pure compound will necessarily crystallize in one of the 65 Sohncke space groups. Nonetheless, only 22 of these are chiral space groups. In these 22 cases, point inversion transforms one space group into its enantiomorphic partner. For instance, $P6_1$ transforms into $P6_5$ and *vice versa*. When the Sohncke space group is achiral, inversion through a point does not transform the space group, for example space group $P2_1$. Therefore, to sum up, just 22 space groups are chiral, but 65 space groups are allowed for chiral molecules. A classification of all the space groups is presented in Table 2.

Table 2. Classification of the crystallographic space groups.

Centrosymmetric space groups
$P\bar{1}$, $P2/m$, $P2_1m$, $P2/c$, $P2_1c$, $C2/m$, $C2/c$, $Pmmm$, $Pnnn$, $Pccm$, $Pban$, $Pmma$, $Pnna$ $Pmna$, $Pcca$, $Pbam$, $Pccn$, $Pbcm$, $Pnnm$, $Pmmm$, $Pbcn$, $Pbca$, $Pnma$, $Cmmm$, $Cmcm$, $Cmca$, $Cccm$, $Cmma$, $Ccca$, $Fmmm$, $Fddd$, $Immm$, $Ibam$, $Ibcm$, $Imma$, $P\bar{3}$, $R\bar{3}$, $P\bar{3}1m$, $P\bar{3}1c$, $P\bar{3}m1$, $P\bar{3}c1$, $R\bar{3}m$, $R\bar{3}c$, $P6/m$, $P6_3/m$, $P6/mmm$, $P6/mcc$, $P6_3/mcm$, $P6_3/mmc$, $Pm\bar{3}$, $Pn\bar{3}$, $Pa\bar{3}$, $Fm\bar{3}$, $Fd\bar{3}$, $Im\bar{3}$, $Ia\bar{3}$, $Pm\bar{3}m$, $Pn\bar{3}n$, $Pm\bar{3}n$, $Pn\bar{3}m$, $Fm\bar{3}m$, $Fm\bar{3}c$, $Fd\bar{3}m$, $Fd\bar{3}c$, $Im\bar{3}m$, $Ia\bar{3}d$, $P4/m$, $P4_2/m$, $P4/n$, $P4_2/n$, $I4/m$, $I4_1/a$, $P4/mmm$, $P4/mcc$, $P4/nbm$, $P4/nnc$, $P4/mbm$, $P4/mnc$, $P4/nmm$, $P4/ncc$, $P4_2/mmc$, $P4_2/mcm$, $P4_2/nbc$, $P4_2/nnm$, $P4_2/mbc$, $P4_2/mcm$, $P4_2/nmc$, $P4_2/ncm$, $I4/mmm$, $I4/mcm$, $I4_1/amd$, $I4_1/acd$.
Non-centrosymmetric and non-Sohncke space groups
Pm, Pc, Cm, Cc, $Pmm2$, $Pmc2_1$, $Pcc2$, $Pma2$, $Pca2_1$, $Pnc2$, $Pmn2_1$, $Pba2$, $Pna2_1$, $Pnn2$, $Cmm2$, $Cmc2_1$, $Ccc2$, $Amm2$, $Abm2$, $Ama2$, $Aba2$, $Fmm2$, $Fdd2$, $Imm2$, $Iba2$, $Ima2$, $P31m$, $P31c$, $P3m1$, $P3c1$, $R3m$, $R3c$, $P\bar{6}$, $P6mm$, $P6cc$, $P6_3cm$, $P6_3mc$, $P\bar{6}m2$, $P\bar{6}c2$, $P\bar{6}2m$, $P62c$, $P\bar{4}3m$, $P\bar{4}3n$, $F\bar{4}3m$, $F\bar{4}3c$, $I\bar{4}3m$, $I\bar{4}3d$, $P\bar{4}$, $I\bar{4}$, $P4mm$, $P4bm$, $P4_2cm$, $P4_2nm$, $P4cc$, $P4nc$, $P4_2mc$, $P4_2bc$, $I4mm$, $I4cm$, $I4_1md$, $I4_1cd$, $P\bar{4}2m$, $P\bar{4}2c$, $P\bar{4}2_1m$, $P\bar{4}2_1c$, $I\bar{4}2m$, $I\bar{4}2d$, $P\bar{4}m2$, $P\bar{4}c2$, $P\bar{4}b2$, $P\bar{4}n2$, $I\bar{4}m2$, $I\bar{4}c2$.
Achiral Sohncke space groups
$P1$, $P2$, $P2_1$, $C2$, $P222$, $P222_1$, $P2_12_12$, $P2_12_12_1$, $C222$, $C222_1$, $F222$, $I222$, $I2_12_12_1$, $P3$, $R3$, $P312$, $P321$, $R32$, $P6$, $P622$, $P6_322$, $P23$, $P2_13$, $F23$, $I23$, $I2_13$, $P432$, $P4_332$, $F432$, $F4_132$, $I432$, $I4_132$, $I4$, $I4_1$, $P422$, $I422$, $I42_12$, $P4$, $P6_3$, $P4_2$, $P42_12$, $P4_222$, $P4_22_12$.
Chiral Sohncke space groups
$P4_1/P4_3$, $P4_122/P4_322$, $P4_12_12/P4_32_12$, $P3_1/P3_2$, $P3_121/P3_221$, $P3_112/P3_212$, $P6_1/P6_5$, $P6_122/P6_522$, $P6_2/P6_4$, $P6_222/P6_422$, $P4_132/P4_232$.

3. Evaluation of absolute structure and configuration

Absolute structure is a crystallographer's term and is defined as the spatial arrangement of the atoms of a physically identified non-centrosymmetric crystal, and is described by way of the unit-cell dimensions, space group, and representative coordinates of all atoms. Absolute configuration of a molecule is a chemist's term and is defined as the spatial arrangement of the atoms of a physically identified chiral molecular entity, and is specified with the corresponding stereochemical description (*S*, *R*, *D*, *L*, Δ, Λ, etc.) and can be determined by examining the chirality sense of the molecule [24]. In dealing with crystal structures, the chirality arising from the molecular components of the crystal and the chirality arising from the space group must be distinguished. As a consequence, absolute structure needs to be considered for any non-centrosymmetric crystal structure, whether in Sohncke space groups or not, and absolute configuration can only be determined in Sohncke space groups.

The distinction between a non-centrosymmetric crystal structure and its inverted image is possible thanks to differences in the intensity of Friedel pairs, (*h*, *k*, *l*) and (−*h*, −*k*, −*l*). This was first demonstrated by Coster et al. in 1930, who showed that the (111) and $(\bar{1}\bar{1}\bar{1})$ reflections of zinc blende have unequal intensities when the wavelength is close to the zinc absorption edge [25]. Before this discovery, the inversion-distinguishing power of X-ray diffraction was considered to be non-existent according to Friedel's law; Friedel himself argued, by using optics and crystal symmetry, that the intensities of the Bragg reflections (*h*, *k*, *l*) and (−*h*, −*k*, −*l*) are always identical regardless of the point group of the crystal [26]. The inequality of the intensity of the Friedel pairs is due to resonant scattering, a change in the phase of the diffracted X-ray for atoms with an absorption edge close to the X-ray wavelength. The

amount of energy that individual atoms absorb depends on their atomic number and light atoms such as carbon, nitrogen, and oxygen do not contribute much to resonant scattering at typical wavelengths used for X-ray crystallography. Thus, the resonant scattering is all the more observable as the crystallized compound contains atoms with high atomic number, Z (heavy atoms in the language of crystallographers). However nowadays, thanks to the development of technologies and methods, tiny resonant scattering signals can be detected, allowing the determination of the absolute structure of crystals containing only light atoms (C, N, O) as developed further in this section. Bijvoet and collaborators achieved the first determination of absolute configuration (that of sodium rubidium tartrate) by X-ray diffraction using dispersive scatterers [27,28].

Until the 1990s, absolute structure determination usually relied on Hamilton's *R*-factor ratio test. The basis of this method is the comparison of the conventional or weighted *R* factors from the refined model of the structure and its inverted structure [29]. However, this test cannot take account of the effects of inversion twinning (a two-domain structure twin whose twins are related to each other by an inversion point). Rogers was the first to introduce, in 1981, a parameter (η) that can be refined as part of the least-squares refinement. This parameter encodes the magnitude and sign of the measured resonant scattering signal measured in units of *f*'', the imaginary component of the complex atomic scattering factor [30]. Two years later, this parameter was superseded by the Flack parameter (x). Flack pointed out that Roger's parameter only had physical meaning at the limiting values ±1 and he suggested that a given crystal could be studied as a crystal containing a mole fraction of a given handedness equivalent to x, and a mole fraction of the other handedness equivalent to $1-x$. Consequently, the x parameter has physical meaning throughout the range 0-1 and takes into account the possible effects of twinning by inversion [31]. Therefore, the Flack parameter is now the principal factor used to estimate the absolute configuration of a structural model, the molar fraction x in the defining equation:

$$C = (1\text{-}x)\, X + x\, \bar{X}$$

where C represents an oriented two-domain-structure crystal twinned by inversion, consisting of an oriented domain structure X and an oriented inverted domain structure $\bar{X}$. In reciprocal space, the Flack parameter x is defined by the structure-amplitude equation:

$$G^2(h, k, l, x) = (1\text{-}x)\, |F(h, k, l)|^2 + x\, |F(\bar{h}, \bar{k}, \bar{l})|^2$$

Depending on the value of the Flack parameter, different conclusions can be reached for the determination of the absolute structure:

1) If $x = 0$ (plus or minus a small standard uncertainty), the absolute structure assigned is most likely correct.

2) If $x = 0.5$ (plus or minus a small standard uncertainty), the crystal may be racemic or an inversion twin.

3) If $x = 1$ (plus or minus a small standard uncertainty), the absolute structure is most likely the inverted one.

Guidelines exist to judge whether the absolute structure has been satisfactorily determined. First, the value of the standard uncertainty (u) of the Flack parameter ($x(u)$) has to be less than 0.04 (although it can be up to 0.10 for a sample proven by other methods to be enantiomerically pure). Second, the value of the Flack parameter should be equal to zero within a region of three standard uncertainties, or, in other words, the relationship between the Flack parameter and its standard uncertainty must be less than 3.0 ($|x|/u$) < 3.0. These criteria were established by statistical reasoning to assure a valid determination of the absolute structure by Flack and Bernardinelli in 2000 [32].

Methods involving the careful recording of intensities of Friedel opposites in such a way that systematic errors are cancelled [33] or even methods in which refinement weights are modified for data in proportion to their sensitivity to the Flack parameter were later developed in order to lower its standard uncertainty [34]. In 2006, Diettrich et al. reported the use of 'invarioms' in the determination of absolute structures. Invarioms are aspherical scattering factors that take into account electron density deformations [35]. Using invarioms instead of the normal spherical scattering factors can somewhat improve the precision of the standard uncertainty in the value of the Flack parameter.

Until recently, the evaluation of absolute structure determination has been based entirely on the values of parameters derived from least-squares like the Flack parameter, but little attention was paid to the fit of the model to the observed diffraction intensities. In 2008, Hooft introduced a new method to determine the absolute structure of a crystal, based on Bayesian statistics applied to the Bijvoet differences [36]. Given different hypotheses for the absolute structure the probability distribution of all observed Bijvoet pairs is calculated and the solution with the highest probability can be determined. Moreover, the outcome of the analysis can be cast in the form of a value with standard uncertainty that can be compared to the Flack parameter. With this method (improved later in 2010 [37]), providing that the largest possible number of Bijvoet pairs has been measured, the absolute structure of crystals containing only light atoms can also be assessed even in the case of an unoptimized X-ray source (e.g. at the Mo wavelength) [38]. In 2011 Watkin established that plots of D_{obs} vs. D_{model}, where D is the difference in intensity between Friedel pairs, can be employed as a data evaluation technique [39]. Moreover, from this plot the Flack parameter and its standard uncertainty can be obtained. In this way, a slope of 1 corresponds to a Flack parameter of 0, and a slope of 0 to a Flack parameter of 0.5 [40,41]. Parsons also introduced the use of intensity quotients and differences of the Bijvoet pairs in absolute structure determination, thus enabling the refinement of the Flack parameter along with all other parameters, though the methods are usually applied post-refinement by default (without correlation with other parameters) in most crystallographic software. The method was proven to give more precise estimates than conventional refinements [42].

For a correct absolute structure determination, it is important to measure pairs of Friedel opposites (*h, k, l*) and (−*h*, −*k*, −*l*) (or symmetry equivalents) and use them separately in the refinement. This is defined by the "Friedel coverage", a measure of the completeness of the diffraction intensity data with regard to inversion in the origin reciprocal space. If for each value of (*h, k, l*) the intensity of the Friedel opposite (−*h*, −*k*, −*l*) (or one symmetry-equivalent to it) has not been measured, the Friedel coverage is 0%. However, if for each value of (*h, k, l*), both the reflection (*h, k, l*) and its Friedel opposite (−*h*, −*k*, −*l*) (or one symmetry-equivalent to it) have been measured and used separately in the least-squares refinement, then the Friedel coverage is 100%. The Friedel coverage must be close to 100% for accurate chirality determination in a new crystal structure [43].

The capacity to achieve a low standard uncertainty for the Flack parameter depends strongly on the resonant scattering effects having sufficient magnitude to lead to measurably different intensities for Friedel pairs of reflections. It is commonly admitted that the most important problem in this regard is the insufficient resonant scattering of light-atom structures. To predict the inversion-distinguishing power for a specific compound and at a specific wavelength, the Bijvoet intensity ratio (χ) can be calculated just from the composition of the crystal and the corresponding wavelength:

$$\chi = \frac{\sqrt{<D^2>}}{<A>}$$

Where:

$$A(hkl) = ½\ [I(hkl) + I(\bar{h}\bar{k}\bar{l})]$$

$$D(hkl) = [I(hkl) - I(\bar{h}\bar{k}\bar{l})]$$

This is normally presented in values of $10^4\chi$, and this product is denoted $\text{Friedif}_{\text{stat}}$ [44–47]. On the basis of empirical trends extrapolated from published values of x and its uncertainty, refined in the conventional manner (no intensity quotients or differences refinement), it has been established that a value for $\text{Friedif}_{\text{stat}}$ of 200 would corresponds to a standard uncertainty for the Flack parameter of 0.04 and a value for $\text{Friedif}_{\text{stat}}$ of 80 to a standard uncertainty for the Flack parameter of 0.10, the limiting values for an acceptable absolute structure determination. However, the ability to determine absolute structure precisely also depends on low levels of random and systematic errors in intensity measurements [32,42,48].

Two estimates of the Bijvoet ratio are available and their comparison leads to useful information. The first one is the already-mentioned $\text{Friedif}_{\text{stat}}$, which arises from considerations of intensity statistics through the analysis of a structure composed of a random distribution of atoms. The second is denominated $\text{Friedif}_{\text{obs}}$, which is obtained from the observed diffraction intensities [39]. When comparing these two estimations the following conclusions can be obtained [48]:

1) If $Friedif_{obs}$ is much lower than $Friedif_{stat}$, the crystal structure is either centrosymmetric, or non-centrosymmetric with the crystal twinned by inversion in a proportion close to 50:50, and random uncertainties and systematic errors in the intensity data set are minor.

2) If $Friedif_{obs}$ is close in value to $Friedif_{stat}$, then the crystal is non-centrosymmetric, not twinned by inversion, and random uncertainties and systematic errors in the intensity data set are minor. However, data from a centrosymmetric crystal with large random uncertainties and systematic errors may also produce this result.

3) If $Friedif_{obs}$ is much larger than $Friedif_{stat}$, then either the data set is dominated by random uncertainties and systematic errors, or the chemical formula is erroneous.

Only when the absolute structure has been determined satisfactorily is it possible to know whether the absolute configuration of the molecule can be established, since not all valid determinations of absolute structure necessarily lead to the assignment of an absolute configuration [49]. For that:

1) The space group must be a Sohncke space group.

2) One needs to identify the potential molecular unit and its spatial arrangement in the crystal structure, and then examine that it has not any roto-inversion or roto-reflection symmetry operations. If any of these symmetry operations is found, then the molecule is achiral, and its absolute configuration cannot be determined. For example, any planar molecule has a mirror plane and is achiral no matter whether this plane is part of the space group symmetry or not.

3) In the case of an asymmetric unit containing more than one occurrence of the chiral molecule ($Z' > 1$), one needs to verify that all the molecular entities are the same enantiomer.

Nowadays, the data obtained from crystal structure determination are stored as computer readable files, or *CIF* files, which can be used for display, analysis, evaluation, and archiving of crystal structures. The data-measurement and structure-refinement procedures are archived in the CIF file and can be examined with the aid of the appropriate software. The most elaborate system currently in operation for this evaluation is the free-of-charge online checkCIF/PLATON operated by the International Union of Crystallography [50]. The validation software generates a set of alerts classified as level A, B or C. Level A alerts are due to serious problems in the structure determination and their related problems should be resolved or, exceptionally, convincingly explained. Level B alerts are of an intermediate importance and normally they should be resolved. Level C alerts are generated because non-standard issues and they should be examined to decide whether they can be ignored, or they must be solved. However, large numbers of level B and C alerts should not be ignored, since collectively they could indicate grave problems with the structure solution. The assignment of a wrong space group is one of the most common mistakes in the determination of a crystal structure [51], and checkCIF/PLATON may

warn that a space group of too low symmetry has been chosen. Therefore, the employment of this software is strongly advised for each single crystal structure determination. It is often the case that it is possible to add a center of symmetry to the chosen space group, although this proposition should be rejected if there is strong evidence to show that the compound is enantiomerically pure.

Referring to PLATON, it has also recently been shown that, in favorable cases, the absolute structure of crystals containing atoms with strong resonant scattering in unresolved regions can be recovered. The concept is based on a modified version of the SQUEEZE method implemented in PLATON (SQUEEZE allows to approximate the X-ray scattering of undetermined disordered regions in crystals via a discrete Fourier transform of the residual electron density) through a procedure, called HUG, that constructs a model of the unresolved region in which the resonant scattering contribution is either distributed over the volume of that region or estimated as proportional to the electron density at each point of the volume [52].

4. The extreme versatility of chiral molecular packing: Case studies

In the previous section, the main methods and criteria necessary to correctly determine an absolute structure (non-centrosymmetric crystal) and/or an absolute configuration (Sohncke space group) have been reviewed. If the material studied is a chiral compound with an extremely high degree of enantiopurity, its crystallization will give a batch of homochiral crystals and, respecting the previous recommendations, the interpretation of the data will be easy in terms of absolute structure and configuration. In the case of non-enantiopure chiral compounds things can become seriously complex and make the interpretation of the measured crystal partially accurate with respect to the reality of the bulk, or even in total contradiction. Section 5 on crystal assemblies will come back to this point and the strategies to adopt to overcome this problem, but it is first necessary to interpret the results obtained on a single crystal, which is not always trivial. Indeed, non-enantiopure chiral compounds present a remarkable versatility when they are put in crystallization conditions. The study of Gubaidullin *et al.* on a family of chiral ortho-alkyl phenyl ethers of glycerol illustrates perfectly the problem [53]. By modifying only one substituent on the glycerol moiety (scheme 1) and using various solvents of crystallization, the authors were able to obtain nine different crystal phases representing four different modes of crystallization - conglomerates, racemates, kryptoracemates and anomalous conglomerates - among those possible for a chiral molecule. Other examples of a family of compounds crystallizing in several modes can be found in the literature [54,55].

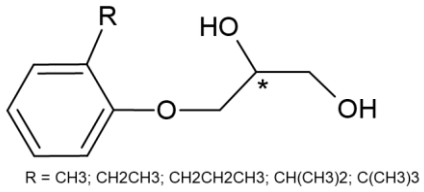

R = CH3; CH2CH3; CH2CH2CH3; CH(CH3)2; C(CH3)3

Scheme 1

These terms, along with the others representing the different crystalline variants of a chiral compound are discussed hereafter and are illustrated by examples from the literature or from our work.

The most common forms of crystallization for a racemic mixture of chiral molecules are pure racemic crystals, with non-Sohncke space group, and conglomerates [56]. In the former case the two enantiomers are present in equal amount in the crystal, with only one independent molecule in the asymmetric unit (Z'=1) and are related in the unit cell by a symmetry operation of the second kind. These crystals represent about 90% of the instances for chiral molecules. In conglomerates the enantiomers crystallize separately in a Sohncke space group and form crystals of opposite handedness. They represent 5-10% of the cases. These two situations are very common and well-known and do not require further comment. The following five crystallization modes are much less common and represent only a small percentage of cases for chiral crystallized molecules. It is nevertheless essential to know how to recognize and characterize them.

When Z' is greater than 1 and takes an even value the crystal is known as a kryptoracemate [57,58], also named 'false conglomerate' [59,60]. The composition of the crystal is purely racemic but the space group is a Sohncke one. Indeed, the two enantiomers co-exist in the asymmetric unit, most commonly as two independent molecules, thanks to some conformational differences, which can be very tiny. One explanation for the propensity of some chiral molecules to crystallize as kryptoracemates is that pseudosymmetric elements within the unit cell would free them from symmetry positional constraints thus optimizing their interactions and allowing a higher efficient packing [60]. The number of kryptoracemates deposited in the organic Cambridge Structural Database has been estimated between about 200 and 400, depending on the date and methodology of search [58,61]. The superimposition of the two enantiomers, after inversion of one of them, can be a simple and efficient way to highlight their differences as illustrated in the figure 2 of [56]. However kryptoramecates with an even Z' > 2 can also be found and for instance Kramer & Bolte could obtain crystals of two very similar compounds [62] differing in just one residue, but both crystallizing in a Sohncke space group with respectively Z' = 2 and Z' = 4 (plus two CH_2Cl_2 solvent molecules in the latter case) as illustrated in Figure 1.

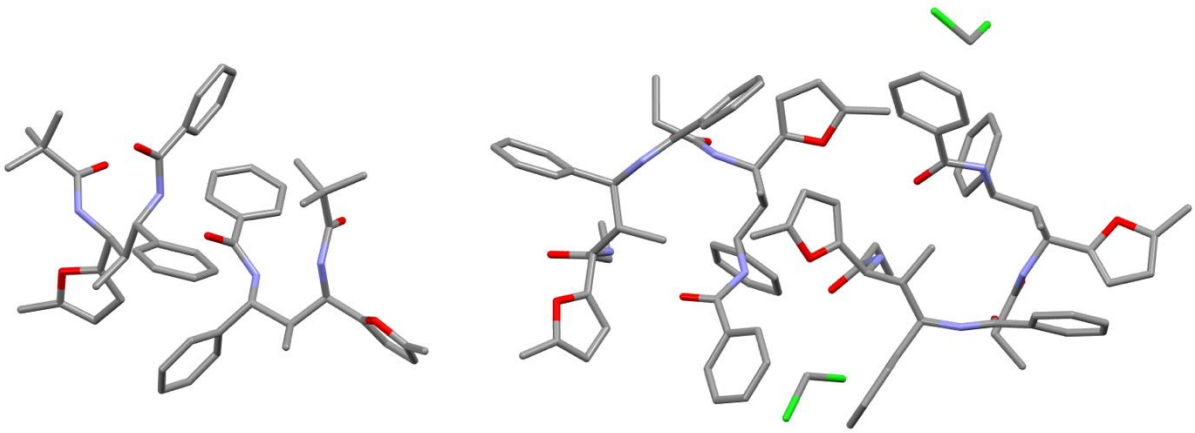

Figure 1. An example of kryptoracemates with even numbers of enantiomers [60]. Left: Z' = 2; right: Z' = 4.

An example from our work is the kryptoracemate formed from the chiral linear tricobalt cluster $[Co_3(dpa)_4(MeCN)_2]^{2+}$ (where dpa = 2,2'dipyridylamine). This cluster is part of a family known as "Extended Metal Atom Chains" (EMACs) [63] or "Metal Strings" [64], which usually have a helical geometry due to the wrapping of the ligands around the metal axis arising from steric hydrogen-hydrogen atom repulsion (Figure 2a,b). In the crystal of $[Co_3(dpa)_4(MeCN)_2](BF_4)_2 \cdot MeCN \cdot 0.5Et_2O$ (**1**), the asymmetric unit contains the two EMAC enantiomers, crystallizing in the space group $P2_12_12_1$. Superposition of the two enantiomers with inversion of one of them shows excellent overlap, except for slight differences in the axial acetonitrile molecule angles (177.69°/178.67° and 177.42°/179.10°), which may account for the conformational uniqueness of the two enantiomers (Figure 2c). Analysis of the space group with PLATON AddSymm did not find any other suitable settings.

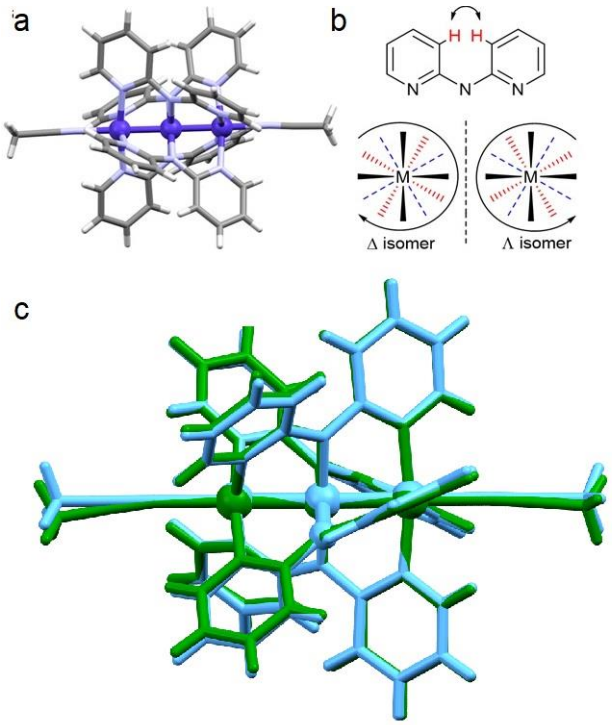

Figure 2. a) Rendering of the $[M(dpa)_4(MeCN)_2]$ cation EMAC, b) Wrapping of dpa ligands around the metal core to form CW (Δ) and CCW (Λ) isomers, c) Superposition of the enantiomers of $[Co(dpa)_4(MeCN)_2]^{2+}$ in the kryptoracemate **1**.

Even less common are the 'unbalanced crystals' [65] obtained in a Sohncke space group for which only a few examples are published [55]. In this case, the composition deviates from a pure racemate. Previously defined as 'anomalous racemates' [66] this mode of crystallization was later renamed 'anomalous conglomerates' in accordance with their stoichiometry [67]. An example of an anomalous racemate from our labs is another compound featuring an EMAC, $[Cr_3(dpa)_4(MeCN)_2](TRISCAS)_2 \cdot 4.17MeCN$ (**2**), which crystallizes in the space group $P1$. The asymmetric unit is large, consisting of three trichromium cations and six tris(catechol)arsenate (TRISCAS) anions, along with several acetonitrile molecules of solvation. In the analyzed crystal, two of the trichromium cations are in the lambda configuration and one is in the delta configuration.

Likewise, four of the TRISCAS anions are in the delta configuration and two are in the lambda configuration. The packing is complicated, consisting of both homochiral and heterochiral interactions, such that the Δ-Cr_3 isomers interact mainly with Δ-TRISCAS, while the Λ-Cr_3 isomers interact with both TRISCAS isomers (Figure 3). This unbalanced arrangement of enantiomers is likely due to the slow racemization of the TRISCAS anion in the reaction media during crystallization. When the crystallization is carried out over a longer time period, true racemic crystals are obtained as the racemization reaches completion.

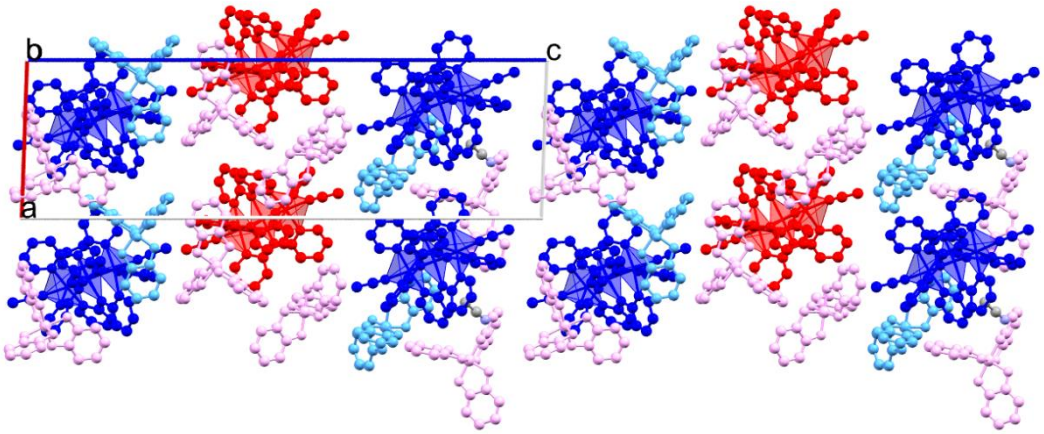

Figure 3. Rendering of the contents of 4 unit cells of **2**. Hydrogen atoms and acetonitrile molecules of crystallization are removed for clarity. Lambda isomer of the Cr_3 EMAC rendered in dark blue, delta Cr_3 isomer in red, lambda TRISCAS in light blue and delta TRISCAS in pink.

At this point, one can already see the diversity of terms used to describe the different modes of crystallization of chiral molecules. If we are speaking only of the proportion of enantiomers in the crystal, general terms like racemates (stoichiometric composition) or scalemates (unbalanced composition) can be used to describe the four previous cases. But as we have seen, the determination of the composition of the asymmetric unit is very important and a more advanced vocabulary should allow a real description of it. In 2012 an attempt in this direction was made by Klika with a very precise classification of chiral systems, including crystals [68]. However, we will continue to use the terms most commonly chosen by the crystallographers to describe the last three cases encountered with crystallized chiral compounds. In this regard the fifth instance that can be presented is that of inversion twin.

Here also a discussion going beyond the purely semantic aspect could be developed because the terms ‘inversion twin’ and ‘racemic twin’ are sometimes used without distinction from each other [69]. But in both cases the chiral molecules crystallize in a non-centrosymmetric space-group, in the form of two domains related by a center of symmetry, each containing only a single enantiomer. The distinction between ‘inversion’ and ‘racemic’ could be related to the ratio of enantiomers present in the crystal, which must be 0.5 in the second case, a ratio that is estimated by the value of the Flack parameter,

providing that all conditions are required like a low uncertainty and the verification of the presence of the anomalous signal (see section 2.2). In that sense, a racemic twin can be seen as a special case of inversion twin and an example of such a crystal is presented below, again involving a trinuclear cluster.

In the literature on EMACs, there is one reported case of spontaneous resolution; the compound $[Co(dpa)_4(MeCN)_2](PF_6)_2$ was found to crystallize, in the same batch, as racemic crystals in the space group $P\bar{1}$ with three molecules of acetonitrile, and as enantiopure species in the space group $P2_1$ with one molecule of acetonitrile and two molecules of diethyl ether (**3**) (Table 3) [70]. We found that the analogous compound $[Co(dpa)_4(MeCN)_2](BF_4)_2 \cdot MeCN \cdot Et_2O$ (**4**) crystallizes in the $P2_1$ space group, with similar unit cell parameters as those found for Δ- and Λ-$[Co(dpa)_4(MeCN)_2](PF_6)_2 \cdot MeCN \cdot 2Et_2O$ (Table 3). However, when the Δ configuration was assigned to the cobalt cluster in the crystal **4a**, the Flack parameter was found to be close to 0.5, and thus the possibility of a racemic twin was examined. Using PLATON we first checked the presence of missed extra symmetry but without success. The Wilson plot[1], generated by Olex2, was totally in accordance with a non-centrosymmetric space-group (Figure 4a), and the plot of the differences D_{obs} vs. D_{model} clearly showed that the data were not dominated by random uncertainty and systematic errors (Figure 4b).[40,41] As discussed in section 2, the slope of the D_{obs} vs. D_{model} being close to zero is indicative of a Flack parameter of 0.5. This structure (**4a**) was thus refined as an inversion twin.

Table 3. Crystal and refinement data for PF_6 (**3**) and BF_4 (**4**) salts of $[Co_3(dpa)_4(MeCN)_2]$ in enantiopure and enantiomerically twinned examples.

	Λ-**3**	Δ-**3**	Δ-**4a**	Δ-**4b**
SG	$P2_1$	$P2_1$	$P2_1$	$P2_1$
T / K	213	163	100	120
A / Å	11.7576(7)	11.721(2)	11.6556(9)	11.5105(5
B / Å	21.9059(6)	21.801(3)	21.914(2)	21.4534(10)
C / Å	12.0621(5)	12.027(5)	11.7175(10)	11.6868(5)
β / deg.	111.883(3)	111.93(2)	113.307(3)	112.875(2)
V / Å^3	2882.9(2)	2850.9(13)	2748.6(4)	2659.0(2)
R1, wR2 all data	0.0445, 0.1160	0.0552, 0.1170	0.0702, 0.1392	0.0344, 0.0838
Flack	-0.01(2)	0.05(2)	0.48(3)	0.008(3)
Ref	[70]	[70]	This work	This work

[1] The Wilson plot is a statistical comparison of the observed intensity data with the theoretical distribution for a random atomic arrangement. The distribution of the normalized diffraction intensities is characteristic of either a centrosymmetric or an acentric crystal. The Wilson plot also establishes the overall displacement parameter for the structure and the scale factor for the data. See A. C. G. Wilson, *Acta Cryst.*, **1949**, *2*, 318.

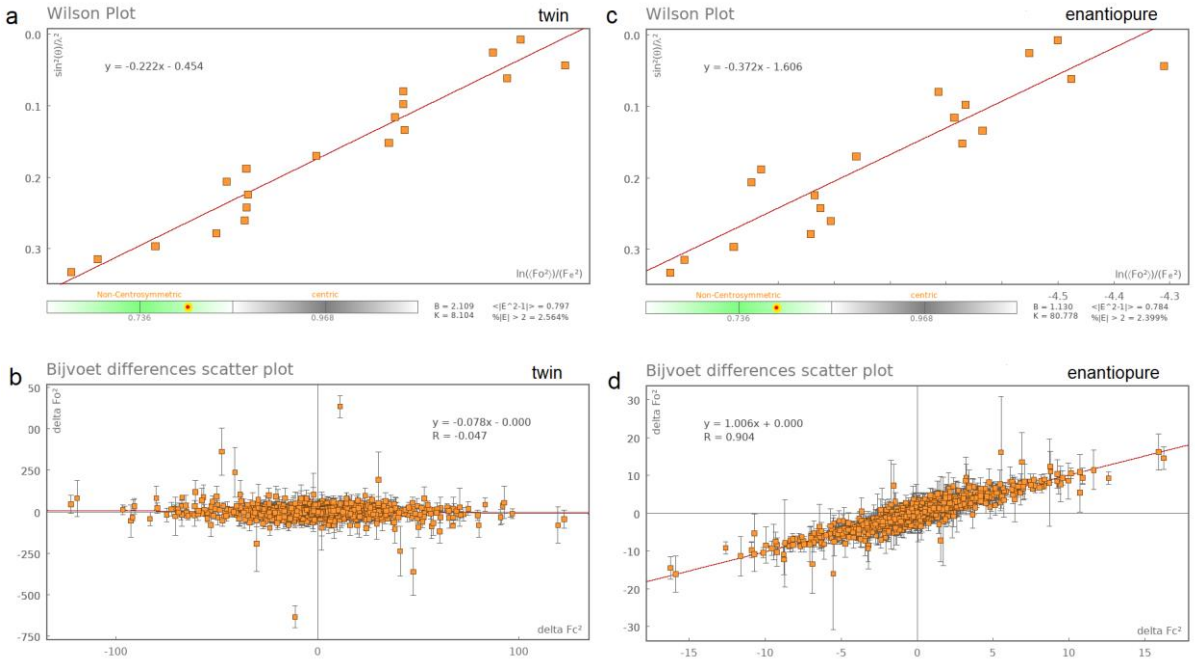

Figure 4. Reflection statistics for (a,b) enantiomerically twinned (**4a**) and (c, d) enantiopure (**4b**) $[Co(dpa)_4(MeCN)_2](BF_4)_2 \cdot MeCN \cdot Et_2O$.

From another crystallization batch was found a crystal of $[Co(dpa)_4(MeCN)_2](BF_4)_2 \cdot MeCN \cdot Et_2O$, but this time with a Flack parameter equivalent to zero (**4b**, Table 3); The difference D_{obs} vs. D_{model} plot clearly validates the choice of the right absolute structure, with a slope equal to 1 (Figure 4d). This further supports the analysis of the previous crystal as a racemic twin, rather than a space group error.

The last two cases represent extreme cases, with Flack parameters of 0.5 and 0. However, an inversion twin can have any composition, and therefore any value of the Flack parameter. An illustrative example of this is the series of $[Fe(phen)_3](TRISCAS)_2$ compounds, which crystallize in the Sohncke space group *R*32. Depending on the optical purity of the chiral anion, the Flack parameters were found to lie between 0 and 0.5 [71]: 0.473(15) with *rac*-TRISCAS, 0.277(2) for Λ-TRISCAS, and two different values of 0.163(13) and -0.006(3) for Δ-TRISCAS. As seen in Figure 5, slopes of the D_{obs} vs. D_{model} plots allow one to derive values of the Flack parameters that are in perfect agreement with values resulting from the structure refinement [42]. This agreement validated the hypothesis of non-racemic inversion twins.

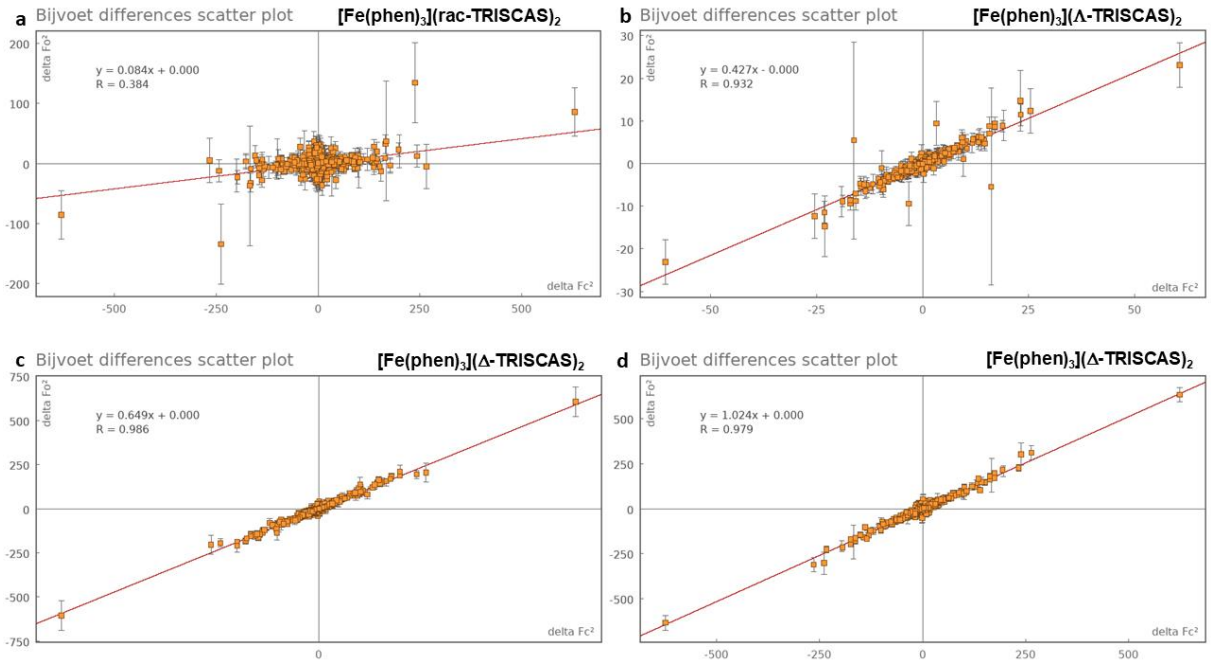

Figure 5. Reflection statistics for (a), $[Fe(phen)_3](rac\text{-}TRISCAS)_2$, (b) $[Fe(phen)_3](\Lambda\text{-}TRISCAS)_2$ and (c, d) $[Fe(phen)_3](\Delta\text{-}TRISCAS)_2$. Flack parameters approximated from the plots slope as (1-slope)/2 were respectively 0.458, 0.286, 0.1755 and -0.012.

The last case of crystalline variants encountered with chiral molecules is the solid solution of enantiomers. Solid solutions are multicomponent materials whose phases are characterized by a structural disorder [72,73]. Their stoichiometry is not limited to a single integral value but can vary on a continuum [74]. A special case are solid solutions of enantiomers that are, however, known to be uncommon. Indeed, it is estimated that only 1-2% of racemic mixtures crystallize as enantiomeric solid solutions [73,75] and at first sight only 25 of them have been fully structurally characterized [76]. Moreover their description and categorization have been subject to debate, but in light of new studies, a tentative classification was recently introduced [76]. In type I enantiomeric solid solutions there is no preferred layout of the enantiomers, which are distributed arbitrarily within the crystallographic molecular positions, which are thus non-stereospecific. Each molecular site can therefore be occupied equally by one or the other enantiomer. Type II solid solution are more complicated to define than type I and they are presented as 'crystalline phases where both enantiomers are largely recognized as different entities upon the formation of the crystal structure'. Thus there is a preferred layout of enantiomers but the crystallographic molecular positions are not fully stereospecific, but enantioselective (see [76] for more details and examples on both solid solution types). It is interesting to note that, in the absence of identification or clear classification, some crystals that were described with generic terms such as 'enantiomeric disorder' could be now be considered as representatives of solid solution classes [77,78].

Hereafter we illustrate two cases of solid solutions from our work. The first example is again linked to the linear metallic clusters and it can be classified as a type I solid solution. These compounds are

polymers consisting of $[Co_3(dpa)_4]^{2+}$ and $M^{IV}F_6^{2-}$ building units, where M^{IV} = Re, Sn, Zr, Os and Ir [79,80]. The enantiomers alternate along the chain direction, so that the polymer itself is not chiral, and the materials crystallize in the centrosymmetric space group P4/ncc. Nonetheless, this provides an interesting example of enantiomeric disorder, as each tricobalt position is occupied by both a lambda and a delta isomer (Figure 6). This disorder is general for all of the MF_6 polymers, with major occupancy ranging from about 60% to 80%.

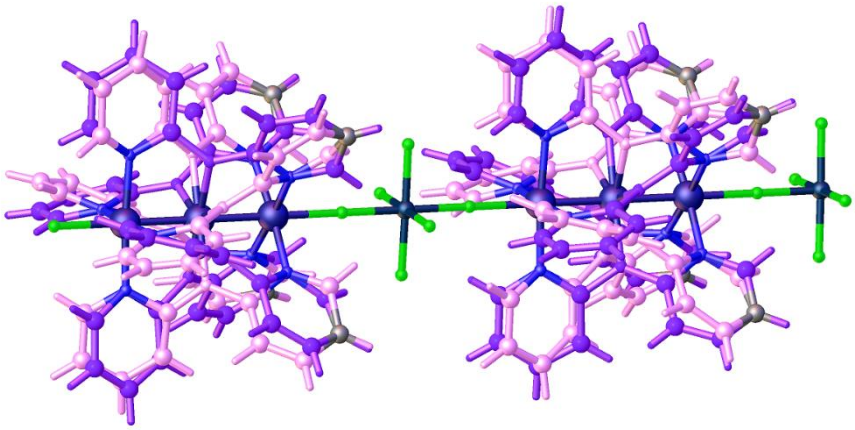

Figure 6. Section of the $[Co_3(dpa)_4](IrF_6)$ polymer from ref [80]. Major part (62%) is shown in purple, minor part (38%) in pink; carbon atoms belonging to both parts shown in gray. While both enantiomers sit on the same position, the major handedness changes from cluster to cluster.

A stranger and more disturbing case is presented hereafter. As part of Ph.D. work on the control of chirality in organic synthesis [81] Sasso d'Elia synthesized a chiral bis-dihydrofuran derivative **5** presenting an unstable configuration at room temperature (low barrier of enantiomerization). However, in order to characterize the molecule, we crystallized it in dichloromethane and obtained beautiful prisms too large to be analyzed by single crystal X-ray diffraction. We thus cut a piece of adequate size (0.25 x 0.25 x 0.35 mm^3), performed the analysis, and solved the structure in the Sohncke space group $P2_12_12_1$, with the molecule in a helical P configuration, as revealed without ambiguity by the Flack and Hooft parameters as well as by the presence of the anomalous signal in the data (Table 4 and Figure 7).

Table 4. Crystal and refinement data for P and M helicenes.

	6P	**6M**
SG	$P2_12_12_1$	$P2_12_12_1$
T	295 K	295 K
a	8.84690(6) Å	8.84183(13)Å
b	13.14771(9) Å	13.15020(18) Å
c	15.68030(10) Å	15.6622(2) Å
V	1823.88(2)$Å^3$	1821.07(4) $Å^3$
R1, wR2 all data	0.0261, 0.0695	0.0267, 0.0718
Flack	-0.06(5)	-0.04(8)
Bayesian statistics: Coverage Bijvoet pairs (%) Y (Hooft) P2(true) P3(false)	 99 -0.08(4) 1. 0.3E-142	 95 -0.08(6) 1. 0.4E-62

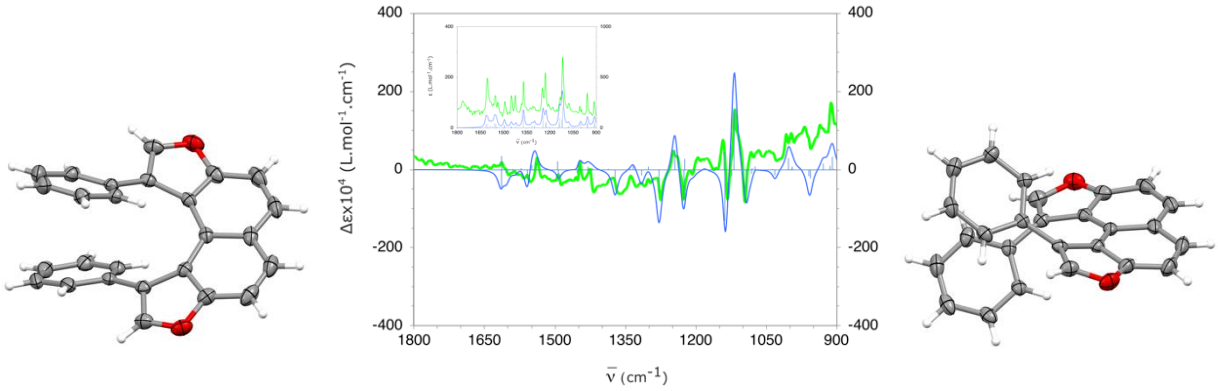

Figure 7. Left: SCXRD structure for **5P**; Middle: experimental (green: measured in KBr pellet) and simulated (blue: calculated at the B3LYP/6-311G(d,p) level) solid state VCD spectra for **5M**. Insert: experimental and simulated IR spectra for **5M**; Right: SCXRD structure for **5M**

In parallel, another piece of the original crystal was analyzed by vibrational circular dichroism (VCD) but the attribution of the absolute configuration was undoubtedly characterized as the complete opposite, the M configuration (**5M** Figure 7). In order to confirm the first SCXRD results we cut another piece from the crystal 'source' and the analysis revealed again and clearly the P configuration for the helicene. A third cut was performed and a new structure obtained, same unit cell and space group as the two previous ones, but this time the absolute configuration was found to be M, without ambiguity, and in accordance with the VCD characterization (Table 4 and Figure 7).

The two enantiomers are also conformers thanks to different torsion angles around the benzyl moieties. In the light of these observations, we first established that we were facing a case of crystallization as an enantiomer solid solution. However according to the characteristics of this latter mode of crystallization as described previously, it seems unlikely that we could obtain pure crystals from each cut and it might be advisable to seek for the right description of the observed phenomenon in another type of crystal packing: a multiple component crystal (discrete variation of the composition) as compared to a solid solution (continuous variation) [74].

In the light of all these examples and the diversity of cases encountered in the crystals of chiral molecules (chiral versatility), it appears essential to remain vigilant when interpreting the absolute structure of a crystal, or the absolute configuration of a molecule. Incorrect or unvalidated conclusions can be easily proposed [82]. It is also essential to ensure the representativeness of the crystal in relation to the bulk, by imaging the entire crystal assembly. Furthermore, as seen in the last example, domain mapping could be useful to differentiate between continuous and multiple component crystals.

5. Crystal assemblies

The previous sections presented SCXRD for the determination of the absolute structure of single crystals. However, a single crystal is not necessarily representative of the crystallization batch, and when

one wishes to determine the chirality of an assembly of crystals, there are very few methods available to do so. In particular, powder X-ray diffraction, which is a technique of choice for ascertaining phase identity in microcrystalline samples, suffers from the drawback of orientational averaging which masks over resonant scattering effects. Only when the sample itself is already biased in such a way as preventing a conglomerate mixture, such as in coordination complexes coordinated with optically pure ligands, can the method be used for ascertaining optical purity in crystal ensembles [83,84]. While the *molecular* enantiomeric excess can be determined by combining the crystals into a single sample, such as the formation of a KBr pellet, and analyzing the material by CD spectroscopy, this technique does not give any information on the *crystalline* enantiomeric excess. This information is crucial when studying, for example, the deracemization of conglomerates by preferential crystallization [85] or attrition methods such as Viedma ripening [86] or Temperature Cycling Induced Deracemization [87]. Since these crystallization techniques rely, at least partially, on secondary nucleation and Ostwald ripening, it is the number of crystals of a given configuration that is of interest, not the overall molecular proportions.

For the chiral determination of individual crystals in a batch, one of the most commonly used techniques is polarized optical microscopy (POM). Many of the studies on deracemization mechanisms have used this method, as it is simple and direct, involving only the turning of a polarizer to differentially change the visual aspect (color, contrast…) of the two different enantiomorphic crystals. However, this technique is mainly limited to transparent crystals, as the measurements are performed in transmission. Furthermore, adulteration by linear birefringence and dichroism limit this technique to cubic crystals, when using unoriented samples [88]. Thus, highly colored or anisotropic crystals are not readily suitable, and for this reason, most deracemization studies using POM have been undertaken on sodium chlorate or bromate [89–94].

There exist other microscopic techniques, which are also limited to certain materials. We can mention second harmonic generation microscopy, which has revealed the handedness of plasmonic materials [95] and chiral surfaces [96]. On the nanoscale, chirality determination has been done using scanning force microscopy on supercoiled DNA plasmids [97], and other supramolecular structures, recently in conjunction with machine learning [98]. As previously mentioned, diffraction using electron microscopy has proven to be able to determine the handedness of crystals [18,99–101], but so far, this technique is limited to single crystals and not crystallization batches. Circular dichroism or polarimetry in conjunction with microscopy has been widely used for imaging chiral thin films and nano-objects. Mueller matrix microscopy, which also allows the deconvolution of the four components of circularly polarized light with chiral matter (linear and circular birefringence and dichroism), has been developed by different research groups [88,102–104]. High Accuracy Universal Polarimetry (HAUP) instrumentation, developed by Japanese researchers, allows the direct determination of the four components,[88,105,106] and this technology has been adapted to perform imaging of crystals, called

scanning-HAUP with a resolution of about 30 μm [3]. Other microscopy experimental set-ups to reduce the impact of linear dichroism have been implemented [107,108]. Circular dichroism studies on chiral thin films have been performed at the B23 beamline [109] at the Diamond Synchrotron [110–115] with a resolution as good as 50 μm. On a smaller scale, CD scattering has been used to determine the chirality of different individual plasmonic gold nano-objects [116–118]. Notably, a microscopy technique using circularly polarized luminescence has been reported for imaging the handedness of nanocrystals [119]. This technique takes advantage of the high emission dissymmetry of Eu(III) ions, which are doped into $TbPO_4 \cdot D_2O$ nanocrystals.

One of the most promising techniques for the study of individual crystals and assemblies is the extension of Natural Circular Dichroism to the X-ray range, XNCD. Expressed as the difference of absorption spectra of right- and left-circularly polarized X-rays around a given absorption edge, this technique profits from the inherent element selectivity, and is sensitive to the chromophore electronic structure (oxidation state, coordination number and geometry). It shares with the more familiar electronic natural circular dichroism the fact of being observable only in non-centrosymmetric media. But due to a different mechanism than ECD, where XNCD optical activity arises mainly from electric dipole-electric quadrupole interference, observing XNCD requires crystals belonging to one of 13 non-centrosymmetric crystal classes [120], some of which ($\bar{4}2m, \bar{4}, mm2, m$) are not active in ECD (and vice versa for 432 and 23, which are ECD active but XNCD-inactive). XNCD was first experimentally observed only recently, in 1998, at the ID12 beamline at the European Synchrotron Radiation Facility [121,122]. The ID12 beamline features high-performance helical undulators insertion devices, providing very stable polarizations in the hard X-ray range (2-20 keV), that allow to measure XNCD either at the metal K-edge for first row transition metals [123–126], or at the L-edges for heavier atoms [121,122,127,128]. Samples are typically measured in total fluorescence yield mode, using photodiodes as detectors oriented in a backscattering geometry: this configuration is specifically interesting since it limits adulteration of the spectra by linear and circular birefringence contributions [125], which are already made weaker by refraction indices in the X-ray range typically very close to unity.

It is of note that XNCD measurements can be performed on either transparent or optically dense crystals. This has led to the development of a new chiral mapping technique, using the XNCD signal. A pioneering study dealt with coordination compounds $[Co(en)_3](NO_3)_2$ and $[Ni(en)_3](NO_3)_2$ [129], which crystallize as conglomerates in space group $P6_322$. Preliminary measurements at the transition metal K absorption edge, performed on single crystals of opposite handedness, which were duly identified through full X-ray diffraction data collection, showed very strong dichroic behavior in the pre-edge features. The dichroic peaks measured at fixed energies determined by these spectra (XNCD maxima were observed at 7712.4 eV for Co and 8335.3 eV for Ni) were then shown to provide directly the handedness of the crystal volume irradiated by the synchrotron X-ray beam spot (Figure 8). Assemblies of 128 crystals of $[Co(en)_3](NO_3)_2$ and 92 crystals of $[Ni(en)_3](NO_3)_2$, mounted with the hexagonal axis

perpendicular to the beam (orthoaxial orientation), were thus mapped using a beam spot size restricted to 150(H)×50(V) μm^2, at the pre-edge XNCD energy maximum, by alternating the circular polarization between right and left [129]. This mapping readily showed that most crystals were effectively composed of a single domain of a given handedness. Nevertheless, the spatial resolution of the technique evidenced two interesting points (Figure 8). On the first hand, a few crystals of $[Ni(en)_3](NO_3)_2$ appeared as neither Δ or Λ down to the spatial resolution of the experiment at the time, suggesting their being truly racemic crystals, an unexpected result for a system supposed to be a conglomerate. On the second hand, other crystals appeared as twinned, with two or three coexisting domains of a given handedness with large borders respective to the beam spot size, but with differences between the two coordination complexes that were suggestive of differences in the crystallization process.

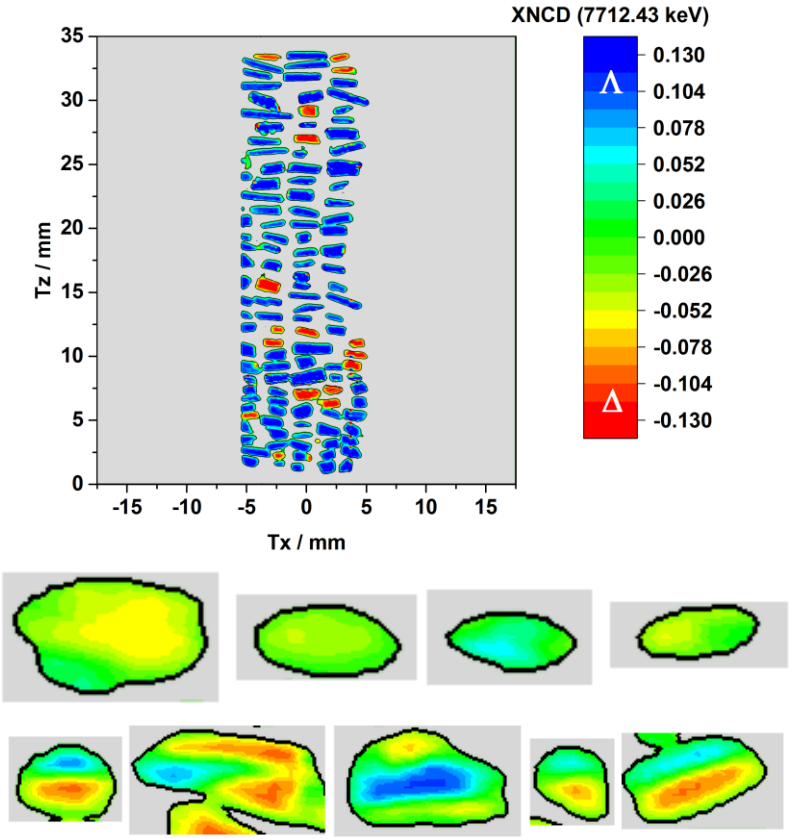

Figure 8. (top) XNCD mapping of an assembly of 128 crystals of $[Co(en)_3](NO_3)_2$. (middle) details of XNCD mapping for racemic crystals and (bottom) twinned crystals of $[Ni(en)_3](NO_3)_2$. From ref [129].

This XNCD domain mapping was shown even more recently to be of use for imaging twin domains in a crystal of the multiferroic $SmFe_3(BO_3)_4$ compound [130]. The compound crystallizes in the *R*32 space group, and crystals were mounted here in the axial configuration, with the trigonal axis along the beam path. Preliminary XNCD spectra at the Fe K-edge showed a strong signal between 5.10^{-3} and 10^{-2} localized at the pre-edge. After setting the beam energy at the maximum found for XNCD and using a

beam spot size of only 43(H)×55(V) μm^2, twinning could be imaged in an overall racemic crystal, with each domain linked to a corresponding enantiomorphous form (Figure 9). Typical domain sizes were seen to be much larger than the beam spot size, typically several hundred μm. Moreover, the respective orientations of the domains given by the mapping allowed the authors to conclude that they were essentially twins by merohedry, characterized by {110} indexing planes, a conclusion that was not readily accessible by conventional X-ray diffraction techniques. This understanding is key towards understanding the external factors giving rise to twinning during the growth of crystals of this compound, and ultimately controlling/inhibiting the growth of twinned domains.

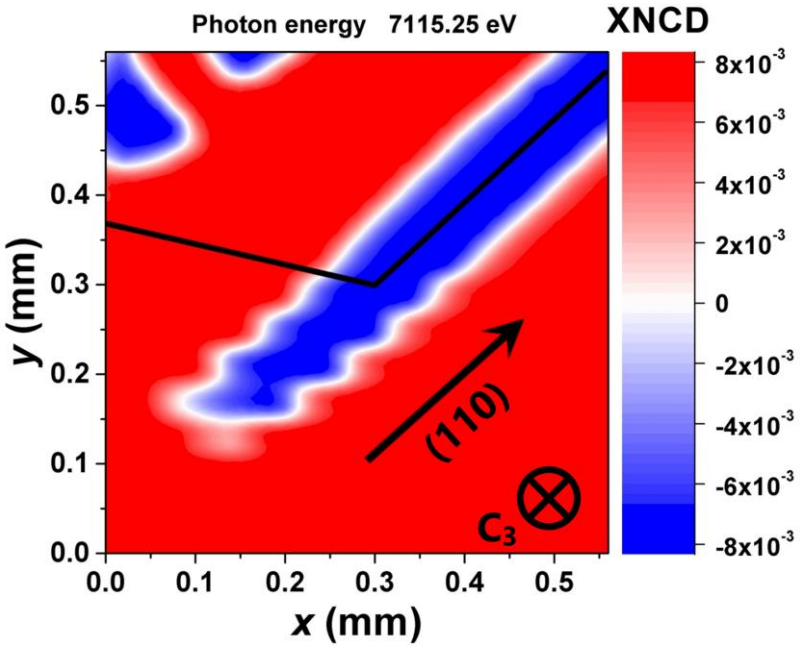

Figure 9. (top) XNCD mapping at room temperature of a racemic crystal of the multiferroic $SmFe_3(BO_3)_4$ compound. From ref [130].

A relevant point is the quantitative nature of XNCD. Indeed, like ECD, if one has an enantiopure reference available, then normalization of the XNCD signal will give a reference value at the energy at which mapping will be performed. Performing the same normalization for the mapping will give normalized values which by comparison to the reference yield directly the enantiomeric fraction for the volume probed by the beam spot. This normalization requires to perform the same mapping twice more, setting the beam at energies before the pre-edge and well above the edge. For lack of time, this normalization procedure was not performed in both cases reported.

Last but not least, the possible extension of XNCD mapping to the K edges of lighter elements would be of course of interest. As XNCD transitions are from core levels to empty levels delocalized around the absorbing atom, both immediate symmetry and the local environment can be probed. Nevertheless,

K edges of light elements (C, O, N) are notoriously difficult to observe correctly at synchrotron beamlines, simply because those atoms constitute most of the residual impurities in the high-vacuum lines, adsorbing on most surfaces including mirrors and monochromators, and thus representing a huge drawback for the high signal stability needed for the observation of XNCD. This accounts for XNCD observation having been limited so far to heavier elements.

6. Closing comments

As evidenced in this review and numerous other texts, X-ray diffraction is a powerful and indispensable tool to study chirality in the solid state for crystalline compounds. Nevertheless absolute structure and/or configuration determination are shown to be sometimes not so straightforward, which we illustrated through a series of 'pathological' cases: kryptoracemates (or 'false conglomerates'), anomalous conglomerates, racemic and inversion twinning, enantiomeric solid solutions. Such a variety of behaviours makes it essential to keep a certain amount of caution and critical eye when interpreting the absolute structure of a crystal, or the absolute configuration of a molecule. Moreover, such interpretations are heavily dependent on the representativeness of the crystal analyzed in relation to the bulk. Accordingly, we presented a new technique, based on X-ray Natural Circular Dichroism, that allows mapping the chirality of an entire assembly of crystal, down to the micrometer scale. Mapping of the components of a given single crystal was demonstrated.

Acknowledgments. The authors would like to thank Drs. C. Sasso d'Elia and D. Bonne (*Aix Marseille Univ, CNRS, Centrale Marseille, ISM2, Marseille, France*) for the synthesis of and Dr. J.-V. Naubron (*Aix Marseille Univ, CNRS, Centrale Marseille, Spectropole FR1739, Marseille, France*) for the IR & VCD analysis of the helicene discussed in the case studies. Anandi Srinivasan for the synthesis of **4b**, Vladimir Bulicanu for the synthesis of **2**, Ahmad Naim and Elen Duverger-Nédellec for the synthesis of the $[Fe(phen)_3](TRISCAS)_2$ series, the University of Bordeaux for the thesis of AVP, the region Nouvelle Aquitaine, the CNRS and the ESRF (beamtime CH-5531).

The data that support the findings of this study are openly available as structures deposited at the Cambridge Structural Database (reference numbers 092344 to 2092349), and can be requested online.

7. References

1. H. Kuang, C. Xu, Z. Tang, *Adv. Mater.*, 32 (2020) 2005110.
2. M. Hwang, B. Yeom, *Chem. Mater.*, 33 (2021) 807–817.
3. W. Kaminsky, K. Claborn, B. Kahr, *Chem. Soc. Rev.*, 33 (2004) 514–525.
4. R. Kuroda, Eng. Cryst. Mater. Prop., Springer, (2008), pp. 251–270.
5. T. Wenzel, J. Wilcox, *Chirality*, 15 (2003) 256–70.
6. T. Wenzel, C. Chisholm, *Prog. Nucl. Magn. Reson. Spectrosc.*, 59 (2011) 1–63.
7. M.J. Potrzebowski, A. Jeziorna, S. Kaźmierski, *Concepts Magn. Reson. Part A*, 32A (2008) 201–218.
8. V. Simonet, M. Loire, R. Ballou, *Eur. Phys. J. Spec. Top.*, 213 (2013).
9. I.A. Zobkalo, *Crystallogr. Rep.*, 66 (2021) 216–230.
10. R. Bau, I. Brewer, M.Y. Chiang, S. Fujita, J. Hoffman, M.I. Watkins, T.F. Koetzle, *Biochem. Biophys. Res. Commun.*, 115 (1983) 1048–1052.
11. H.S. Yuan, R.C. Stevens, R. Bau, H.S. Mosher, T.F. Koetzle, *Proc. Natl. Acad. Sci. U. S. A.*, 91 (1994) 12872–12876.
12. T. Metzenthin, A. Schreiber, R.K. McMullan, T.F. Koetzle, H.S. Mosher, R. Bau, *J. Org. Chem.*, 62 (1997) 5017–5022.
13. M. Yousufuddin, R. Bau, Encycl. Inorg. Chem., American Cancer Society, (2008).
14. J. Jansen, D. Tang, H.W. Zandbergen, H. Schenk, *Acta Crystallogr. A*, 54 (1998) 91–101.
15. A.P. Dudka, A.S. Avilov, G.G. Lepeshov, *Crystallogr. Rep.*, 53 (2008) 530–536.
16. M. Gemmi, E. Mugnaioli, T.E. Gorelik, U. Kolb, L. Palatinus, P. Boullay, S. Hovmöller, J.P. Abrahams, *ACS Cent. Sci.*, 5 (2019) 1315–1329.
17. L. Palatinus, C.A. Corrêa, G. Steciuk, D. Jacob, P. Roussel, P. Boullay, M. Klementová, M. Gemmi, J. Kopeček, M.C. Domeneghetti, F. Cámara, V. Petříček, *Acta Crystallogr. Sect. B Struct. Sci. Cryst. Eng. Mater.*, 71 (2015) 740–751.
18. Z. Dong, Y. Ma, *Nat. Commun.*, 11 (2020) 1588.
19. P. Brázda, L. Palatinus, M. Babor, *Science*, 364 (2019) 667–669.
20. A. Winkelmann, G. Nolze, *Ultramicroscopy*, 149 (2015) 58–63.
21. International Union of Crystallography, *Acta Crystallogr. A*, 55 (1999) 565–600.
22. W.H. Bragg, W.L. Bragg, *Proc. R. Soc. Lond. Ser. Contain. Pap. Math. Phys. Character*, 88 (1913) 428–438.
23. L. Sohncke, Entwickelung Einer Theorie Der Krystallstruktur, Leipzig Teubner, (1876).
24. H.D. Flack, *Helv. Chim. Acta*, 86 (2003) 905–921.
25. D. Coster, K.S. Knol, J.A. Prins, *Z. Für Phys.*, 63 (1930) 345–369.
26. G. Friedel, *CR Acad Sci*, 157 (1913) 1533.
27. J.M. Bijvoet, *Proc K Ned Akad Wet Ser B*, 52 (1949) 313.

28. A.F. Peerdeman, A.J. van Bommel, J.M. Bijvoet, *Proc K Ned Akad Wet Ser B54* (1951) 16.
29. W.C. Hamilton, *Acta Crystallogr.*, 18 (1965) 502–510.
30. D. Rogers, *Acta Crystallogr. Sect. A*, 37 (1981) 734–741.
31. H.D. Flack, *Acta Crystallogr. Sect. A*, 39 (1983) 876–881.
32. H.D. Flack, G. Bernardinelli, *J. Appl. Crystallogr.*, 33 (2000) 1143–1148.
33. S. Parsons, H. Flack, *Acta Crystallogr. A*, 60 (2004) 61–61.
34. S. Parsons, T. Wagner, O. Presly, P.A. Wood, R.I. Cooper, *J. Appl. Crystallogr.*, 45 (2012) 417–429.
35. B. Dittrich, M. Strumpel, M. Schäfer, M.A. Spackman, T. Koritsánszky, *Acta Crystallogr. A*, 62 (2006) 217–223.
36. R.W.W. Hooft, L.H. Straver, A.L. Spek, *J. Appl. Crystallogr.*, 41 (2008) 96–103.
37. R.W.W. Hooft, L.H. Straver, A.L. Spek, *J. Appl. Crystallogr.*, 43 (2010) 665–668.
38. E.C. Escudero-Adán, J. Benet-Buchholz, P. Ballester, *Acta Crystallogr. Sect. B*, 70 (2014) 660–668.
39. H.D. Flack, M. Sadki, A.L. Thompson, D.J. Watkin, *Acta Crystallogr. A*, 67 (2011) 21–34.
40. S. Parsons, P. Pattison, H.D. Flack, *Acta Crystallogr. A*, 68 (2012) 736–749.
41. H.D. Flack, *Acta Crystallogr. Sect. C*, 69 (2013) 803–807.
42. S. Parsons, H.D. Flack, T. Wagner, *Acta Crystallogr. Sect. B Struct. Sci. Cryst. Eng. Mater.*, 69 (2013) 249–259.
43. H.D. Flack, G. Bernardinelli, D.A. Clemente, A. Linden, A.L. Spek, *Acta Crystallogr. B*, 62 (2006) 695–701.
44. H.D. Flack, G. Bernardinelli, *Acta Crystallogr. A*, 64 (2008) 484–493.
45. H.D. Flack, U. Shmueli, *Acta Crystallogr. A*, 63 (2007) 257–265.
46. U. Shmueli, M. Schiltz, H.D. Flack, *Acta Crystallogr. A*, 64 (2008) 476–483.
47. U. Shmueli, H.D. Flack, *Acta Crystallogr. A*, 65 (2009) 322–325.
48. S. Parsons, P. Pattison, H.D. Flack, *Acta Crystallogr. Sect. A*, 68 (2012) 736–749.
49. H.D. Flack, G. Bernardinelli, *Chirality*, 20 (2008) 681–690.
50. A.L. Spek, *J. Appl. Crystallogr.*, 36 (2003) 7–13.
51. R.E. Marsh, A.I. Spek, *Acta Crystallogr. Sect. B*, 57 (2001) 800–805.
52. R.I. Cooper, H.D. Flack, D.J. Watkin, *Acta Crystallogr. Sect. C Struct. Chem.*, 73 (2017) 845–853.
53. A.T. Gubaidullin, A.I. Samigullina, Z.A. Bredikhina, A.A. Bredikhin, *CrystEngComm*, 16 (2014) 6716–6729.
54. A.A. Bredikhin, Z.A. Bredikhina, D.V. Zakharychev, *Mendeleev Commun.*, 22 (2012) 171–180.
55. I. Bernal, R.A. Lalancette, *Comptes Rendus Chim.*, 18 (2015) 929–934.

56. S. Clevers, G. Coquerel, *CrystEngComm*, 22 (2020) 7407–7419.
57. G.A. Morales, F.R. Fronczek, *Acta Crystallogr. C*, 52 (1996) 1266–1268.
58. L. Fábián, C.P. Brock, *Acta Crystallogr. B*, 66 (2010) 94–103.
59. R. Bishop, M.L. Scudder, *Cryst. Growth Des.*, 9 (2009) 2890–2894.
60. A. Steinberg, I. Ergaz, R.A. Toscano, R. Glaser, *Cryst. Growth Des.*, 11 (2011) 1262–1270.
61. E. Grothe, H. Meekes, R. de Gelder, *Acta Crystallogr. Sect. B*, 73 (2017) 453–465.
62. P. Kramer, M. Bolte, *Acta Crystallogr. Sect. C*, 73 (2017) 575–581.
63. J.F. Berry, Mult. Bonds Met. At., Springer, (2005), pp. 669–706.
64. S.-M. Peng, C.-C. Wang, Y.-L. Jang, Y.-H. Chen, F.-Y. Li, C.-Y. Mou, M.-K. Leung, *J. Magn. Magn. Mater.*, 209 (2000) 80–83.
65. V.G. Albano, P. Bellon, M. Sansoni, *J. Chem. Soc. Inorg. Phys. Theor.* (1971) 2420–2425.
66. J. Jacques, A. Collet, S.H. Wilen, Enantiomers, Racemates, and Resolutions, Krieger Pub., (1994) Malabar, FL.
67. A.A. Bredikhin, Z.A. Bredikhina, V.G. Novikova, A.V. Pashagin, D.V. Zakharychev, A.T. Gubaidullin, *Chirality*, 20 (2008) 1092–1103.
68. K.D. Klika, *Int. J. Org. Chem.*, 2 (2012) 224–232.
69. A. Olczak, Remarks on Racemic Twinning, Inversion Twinning and Absolute Structure, (2016).
70. R. Clérac, F.A. Cotton, K.R. Dunbar, T. Lu, C.A. Murillo, X. Wang, *Inorg. Chem.*, 39 (2000) 3065–3070.
71. A. Naim, Y. Bouhadja, M. Cortijo, E. Duverger-Nédellec, H.D. Flack, E. Freysz, P. Guionneau, A. Iazzolino, A. Ould Hamouda, P. Rosa, O. Stefańczyk, Á. Valentín-Pérez, M. Zeggar, *Inorg. Chem.*, 57 (2018) 14501–14512.
72. A.I. Kitaigorodsky, Mixed Crystals, Springer-Verlag, (1984) Berlin Heidelberg.
73. C. Brandel, S. Petit, Y. Cartigny, G. Coquerel, *Curr. Pharm. Des.*, 22 (2016) 4929–4941.
74. M. Lusi, *Cryst. Growth Des.*, 18 (2018) 3704–3712.
75. T. Rekis, A. Bērziņš, L. Orola, T. Holczbauer, A. Actiņš, A. Seidel-Morgenstern, H. Lorenz, *Cryst. Growth Des.*, 17 (2017) 1411–1418.
76. T. Rekis, A. Bērziņš, *CrystEngComm*, 20 (2018) 6909–6918.
77. G. Ferguson, C. Glidewell, *Acta Crystallogr. C*, 57 (2001) 264–265.
78. K. Chulvi, A.M. Costero, L.E. Ochando, P. Gaviña, *Cryst. Growth Des.*, 15 (2015) 3452–3456.
79. V. Bulicanu, K.S. Pedersen, M. Rouzières, J. Bendix, P. Dechambenoit, R. Clérac, E.A. Hillard, *Chem. Commun.*, 51 (2015) 17748–17751.
80. M. Cortijo, V. Bulicanu, K.S. Pedersen, M. Rouzières, J. Bendix, R. Clérac, E.A. Hillard, *Eur. J. Inorg. Chem.*, 2018 (2018) 320–325.

81. C. Sasso d'Elia, Organocatalyse et Multiple Bond-Forming Transformations (MBFTs) Comme Outils Pour Le Contrôle de La Chiralité, These de doctorat, Aix-Marseille, 2017.

82. A. Linden, *Tetrahedron Asymmetry*, 28 (2017) 1314–1320.

83. N.P. Chmel, S.E. Howson, L.E.N. Allan, J. Barker, G.J. Clarkson, S.S. Turner, P. Scott, *Dalton Trans.*, 39 (2010) 2919–2927.

84. S.E. Howson, P. Scott, *Dalton Trans.*, 40 (2011) 4332–4333.

85. G. Coquerel, K. Sakai, N. Hirayama, R. Tamura (Eds.), Nov. Opt. Resolut. Technol., Springer, (2007) Berlin, Heidelberg, pp. 1–51.

86. L.-C. Sögütoglu, R.R.E. Steendam, H. Meekes, E. Vlieg, F.P.J.T. Rutjes, *Chem. Soc. Rev.*, 44 (2015) 6723–6732.

87. K. Intaraboonrod, T. Lerdwiriyanupap, M. Hoquante, G. Coquerel, A.E. Flood, *Mendeleev Commun.*, 30 (2020) 395–405.

88. A.T. Martin, S.M. Nichols, V.L. Murphy, B. Kahr, *Chem. Commun.* (2021).

89. J.-M. Cruz, K. Hernández-Lechuga, I. Domínguez-Valle, A. Fuentes-Beltrán, J.U. Sánchez-Morales, J.L. Ocampo-Espindola, C. Polanco, J.-C. Micheau, T. Buhse, *Chirality*, 32 (2020) 120–134.

90. D.K. Kondepudi, R.J. Kaufman, N. Singh, *Science*, 250 (1990) 975–976.

91. F.S. Kipping, W.J. Pope, *J. Chem. Soc. Trans.*, 73 (1898) 606–617.

92. C. Viedma, *J. Cryst. Growth*, 261 (2004) 118–121.

93. M. Schindler, C. Brandel, W.-S. Kim, G. Coquerel, *Cryst. Growth Des.*, 20 (2020) 414–421.

94. C. Viedma, G. Coquerel, P. Cintas, T. Nishinaga (Ed.), Handb. Cryst. Growth Second Ed., Elsevier, (2015) Boston, pp. 951–1002.

95. V.K. Valev, A.V. Silhanek, N. Smisdom, B.D. Clercq, W. Gillijns, O.A. Aktsipetrov, M. Ameloot, V.V. Moshchalkov, T. Verbiest, *Opt. Express*, 18 (2010) 8286–8293.

96. M.A. Kriech, J.C. Conboy, *J. Am. Chem. Soc.*, 127 (2005) 2834–2835.

97. B. Samorí, G. Siligardi, C. Quagliariello, A.L. Weisenhorn, J. Vesenka, C.J. Bustamante, *Proc. Natl. Acad. Sci. U. S. A.*, 90 (1993) 3598–3601.

98. J. Li, M. Telychko, J. Yin, Y. Zhu, G. Li, S. Song, H. Yang, J. Li, J. Wu, J. Lu, X. Wang, *J. Am. Chem. Soc.*, 143 (2021) 10177–10188.

99. L. Palatinus, C.A. Corrêa, G. Steciuk, D. Jacob, P. Roussel, P. Boullay, M. Klementová, M. Gemmi, J. Kopeček, M.C. Domeneghetti, F. Cámara, V. Petříček, *Acta Crystallogr. Sect. B Struct. Sci. Cryst. Eng. Mater.*, 71 (2015) 740–751.

100. M.C. di Gregorio, L.J.W. Shimon, V. Brumfeld, L. Houben, M. Lahav, M.E. van der Boom, *Nat. Commun.*, 11 (2020) 380.

101. R. Juchtmans, A. Béché, A. Abakumov, M. Batuk, J. Verbeeck, *Phys. Rev. B*, 91 (2015) 094112.

102. O. Arteaga, M. Baldrís, J. Antó, A. Canillas, E. Pascual, E. Bertran, *Appl. Opt.*, 53 (2014) 2236–2245.

103. Y. Wang, H. He, J. Chang, C. He, S. Liu, M. Li, N. Zeng, J. Wu, H. Ma, *J. Biomed. Opt.*, 21 (2016) 071112.

104. T. Huang, T. Huang, R. Meng, J. Qi, Y. Liu, Y. Liu, X. Wang, X. Wang, Y. Chen, Y. Chen, R. Liao, H. Ma, H. Ma, H. Ma, H. Ma, *Opt. Lett.*, 46 (2021) 1676–1679.

105. J. Kobayashi, Y. Uesu, *J. Appl. Crystallogr.*, 16 (1983) 204–211.

106. J. Kobayashi, Y. Uesu, H. Takehara, *J. Appl. Crystallogr.*, 16 (1983) 212–219.

107. S. Hashiyada, T. Narushima, H. Okamoto, *J. Phys. Chem. C*, 118 (2014) 22229–22233.

108. T. Narushima, H. Okamoto, *Sci. Rep.*, 6 (2016) 35731.

109. R. Hussain, T. Jávorfi, G. Siligardi, *J. Synchrotron Radiat.*, 19 (2012) 132–135.

110. F. Zinna, C. Resta, M. Górecki, G. Pescitelli, L. Di Bari, T. Jávorfi, R. Hussain, G. Siligardi, *Macromolecules*, 50 (2017) 2054–2060.

111. G. Albano, M. Górecki, G. Pescitelli, L.D. Bari, T. Jávorfi, R. Hussain, G. Siligardi, *New J. Chem.*, 43 (2019) 14584–14593.

112. R. Hussain, T. Jávorfi, G. Siligardi, *Front. Chem.*, 9 (2021).

113. D.-M. Răsădean, T.-M. Gianga, T. Jávorfi, R. Hussain, G. Siligardi, G.D. Pantoș, *Molecules*, 25 (2020) 6048.

114. J. Wade, J.N. Hilfiker, J.R. Brandt, L. Liirò-Peluso, L. Wan, X. Shi, F. Salerno, S.T.J. Ryan, S. Schöche, O. Arteaga, T. Jávorfi, G. Siligardi, C. Wang, D.B. Amabilino, P.H. Beton, A.J. Campbell, M.J. Fuchter, *Nat. Commun.*, 11 (2020) 6137.

115. R. Hussain, T. Jávorfi, C.S. Hughes, H. Sriram, R. Lashminarayanan, G. Siligardi, *Symmetry*, 12 (2020) 1847.

116. L.-Y. Wang, K.W. Smith, S. Dominguez-Medina, N. Moody, J.M. Olson, H. Zhang, W.-S. Chang, N. Kotov, S. Link, *ACS Photonics*, 2 (2015) 1602–1610.

117. J. Karst, N. Strohfeldt, M. Schäferling, H. Giessen, M. Hentschel, *Adv. Opt. Mater.*, 6 (2018) 1800087.

118. P. Banzer, P. Woźniak, U. Mick, I. De Leon, R.W. Boyd, *Nat. Commun.*, 7 (2016) 13117.

119. E. Vinegrad, U. Hananel, G. Markovich, O. Cheshnovsky, *ACS Nano*, 13 (2019) 601–608.

120. J. Goulon, C. Goulon-Ginet, A. Rogalev, G. Benayoun, C. Brouder, C.R. Natoli, *J. Synchrotron Radiat.*, 7 (2000) 182–188.

121. L. Alagna, T. Prosperi, S. Turchini, J. Goulon, A. Rogalev, C. Goulon-Ginet, C.R. Natoli, R.D. Peacock, B. Stewart, *Phys. Rev. Lett.*, 80 (1998) 4799–4802.

122. J. Goulon, C. Goulon-Ginet, A. Rogalev, V. Gotte, C. Malgrange, C. Brouder, C.R. Natoli, *J. Chem. Phys.*, 108 (1998) 6394–6403.

123. R.D. Peacock, T. Prosperi, B. Stewart, *Chem. Phys. Lett.*, 444 (2007) 375–378.

124. B. Stewart, R.D. Peacock, L. Alagna, T. Prosperi, S. Turchini, J. Goulon, A. Rogalev, C. Goulon-Ginet, *J. Am. Chem. Soc.*, 121 (1999) 10233–10234.

125. J. Goulon, A. Rogalev, F. Wilhelm, N. Jaouen, C. Goulon-Ginet, C. Brouder, *J. Phys. Condens. Matter*, 15 (2003) S633.

126. R. Sessoli, M.-E. Boulon, A. Caneschi, M. Mannini, L. Poggini, F. Wilhelm, A. Rogalev, *Nat. Phys.*, 11 (2015) 69–74.

127. A.P. Oreshko, B.V. Mill, E.N. Ovchinnikova, A. Rogalev, F. Wilhelm, V.E. Dmitrienko, *Crystallogr. Rep.*, 63 (2018) 158–165.

128. I. Mihalcea, M. Perfetti, F. Pineider, L. Tesi, V. Mereacre, F. Wilhelm, A. Rogalev, C.E. Anson, A.K. Powell, R. Sessoli, *Inorg. Chem.*, 55 (2016) 10068–10074.

129. M. Cortijo, Á. Valentín-Pérez, A. Rogalev, F. Wilhelm, P. Sainctavit, P. Rosa, E.A. Hillard, *Chem. – Eur. J.*, 26 (2020) 13363–13366.

130. M.S. Platunov, I.A. Gudim, E.N. Ovchinnikova, K.A. Kozlovskaya, F. Wilhelm, A. Rogalev, A. Hen, V.Y. Ivanov, A.A. Mukhin, V.E. Dmitrienko, *Crystals*, 11 (2021) 531.